American Mineralogist, Volume 89, pages 257–265, 2004

Composition and $I4/m$-$P4_2/n$ phase transition in scapolite solid solutions

YUSUKE SETO,* NORIMASA SHIMOBAYASHI, AKIRA MIYAKE, AND MASAO KITAMURA

Department of Geology and Mineralogy, Kyoto University, Kyoto, 606-8502, Japan

ABSTRACT

Scapolite is a metamorphic aluminosilicate mineral that can be described by the general formula $(Na,Ca,K)_4(Al,Si)_6Si6O_{24}(Cl,CO_3,SO_4)$. Two common end-members are called marialite ($Na_4ClSi_9Al_3O_{24}$) and meionite ($Ca_4CO_3Si_6Al_6O_{24}$). Variations in scapolite composition can be described by two independent substitutions, $NaSi(CaAl)_{-1}$ and $NaCl(CaCO_3)_{-1}$. Twenty eight natural scapolites in the present study exhibit a range of compositions from X_{EqAn} [(Al–3)/3] = 8% and X_{Me} [Ca/(Na+K+Ca)] = 7% to X_{EqAn} = 82% and X_{Me} = 90%. Several coupled exchange reactions can be identified in some inhomogeneous samples (e.g., $Na_{1.49}SiCl_{0.47}[Ca_{1.44}Al(CO_3)_{0.43}]_{-1}$, $Na_{1.69}SiCl_{0.58}[Ca_{1.55}Al(CO_3)_{0.50}]_{-1}$, $Na_{1.91}SiCl_{0.79}[Ca_{1.75}Al(CO_3)_{0.69}]_{-1}$). The extent of coupling between the two substitutions is controlled by the crystallization environment (P, T, and mineral assemblages).

Electron diffraction patterns suggest that the symmetry of scapolite with X_{Me} up to 18% is $I4/m$, whereas that for intermediate scapolite from X_{Me} = 18% to at least X_{Me} = 90% is $P4_2/n$. Under dark-field observation (g = hkl, $h + k + l$ = odd) using a transmission electron microscope (TEM), the $P4_2/n$ samples have anti phase domains of various sizes, the presence of which provides evidence for an I-P phase transition. A wide compositional range of scapolite solid solutions should have an $I4/m$ symmetry at the time of formation.

INTRODUCTION

The mineral scapolite, $[(Na,Ca,K)_4Al_3(Al,Si)_3Si_6O_{24}(Cl,CO_3,SO_4)]$, is found in a wide variety of metamorphic and igneous rocks that have been altered by interactions with crustal fluids. Scapolite is a potential indicator of the activities of volatile components (e.g., Cl, CO_2, and SO_3) during crustal processes because of its ability to incorporate these volatiles (e.g., Moecher and Essene 1990, 1991; Jiang et al. 1994; Kullerud and Erambert 1999).

Scapolite is a framework silicate mineral consisting of four-membered tetrahedral rings similar to feldspar. Unlike feldspar, however, scapolite has two symmetrically distinct rings and cavities in the tetrahedral network. The larger cavities are occupied by Cl^-, CO_3^{2-} and SO_4^{2-}. The smaller cavities are occupied by Na^+, K^+, and Ca^{2+} in amounts necessary to provide charge balance. Accordingly, the stoichiometry of scapolite solid solution can be given as 3 plagioclase + 1 MA (M = Na^+, K^+, or Ca^{2+}; A = Cl^-, CO_3^{2-}, or SO_4^{2-}). The two common end-members of the series are named marialite (Ma: $Na_4Al_3Si_9O_{24}Cl$) and meionite (Me: $Ca_4Al_6Si_6O_{24}CO_3$), and can be represented as $3NaAlSi_3O_8$ NaCl (3 albite + 1 halite) and $3CaAl_2Si_2O_8{\cdot}CaCO_3$ (3 anorthite + 1 calcite), respectively. Teertstra et al. (1999) reported an additional sulfate-dominant member, silvianite ($Ca_4Si_6Al_6O_{24}SO_4$). Scapolite compositions may be understood easily in terms of a quaternary system of albite–anorthite–halite–calcite, as shown in Figure 1. In this figure, the hatched area in the tetrahedron represents the theoretically possible region for scapolite compositions and is called the "scapolite plane." Two substitutions are generally considered as possible in the scapolite plane: $NaSi(CaAl)_{-1}$, which is a plagioclase-type substitution, and $NaCl(CaCO_3)_{-1}$. However, the relationship between these substitutions is still controversial.

Evans et al. (1969) proposed a substitution trend to describe scapolite solid solutions. They subdivided the scapolite solid solution series into two binary solid solutions involving the exchange of $2NaSi + NaCl (2CaAl + CaCO_3)_{-1}$ for compositions between $Na_4Al_3Si_9O_{24}Cl$ (marialite) and $NaCa_3Al_5Si_7O_{24}CO_3$ (named mizzonite) and the exchange of $NaSi(CaAl)_{-1}$ for compositions between $NaCa_3Al_5Si_7O_{24}CO_3$ (mizzonite) and $Ca_4Al_6Si_6O_{24}CO_3$ (meionite). In contrast, Teertstra and Sherriff (1996, 1997) proposed that two changes in the compositional trend in scapolite solid solution located at $[(Na_{3.4}Ca_{0.6})(Al_{3.6}Si_{8.4})O_{24}]^{+1}$ and $[(Na_{1.4}Ca_{2.6})(Al_{4.7}Si_{7.3})O_{24}]^{+1.9}$ divide the series into three portions.

Rebbert and Rice (1997) reported that the substitution $Na_{2.4}Si_{1.4}Cl \leftrightarrow Ca_{2.4}Al_{1.4}CO_3$ occurs between $[(Na_{3.20}Ca_{0.80})(Al_{3.66}Si_{8.34})O_{24}]Cl_{0.86}(CO_3)_{0.14}$ and $[(Na_{1.15}Ca_{2.85})(Al_{4.89}Si_{7.11})O_{24}]Cl_{0.04}(CO_3)_{0.96}$, in the chemical exchange of scapolite from regional metamorphic rocks in the Wallace formation of northern Idaho. Moreover, Kullerud and Erambert (1999) studied the compositional variation of scapolite from a gabbro-anorthosite in northern Norway, and reported that the exchange reaction is $Na_{1.9}Si_{0.8}Cl \leftrightarrow Ca_{1.9}Al_{0.8}A^{2-}$ between the compositions of $[(Na_{3.10}Ca_{0.90})(Al_{3.87}Si_{8.13})O_{24}]Cl$ and $[(Na_{1.25}Ca_{2.78})(Al_{4.65}Si_{7.31})O_{24}]A^{2-}$, where A^{2-} denotes a divalent anion or anion group. By comparing their exchange reaction with that proposed by Rebbert and Rice (1997), Kullerud and Erambert (1999) suggest that small, but significant, differences occur in scapolite solid solutions from different occurrences. A comprehensive scheme to explain these various

*E-mail: seto@kueps.kyoto-u.ac.jp

TABLE 1. Representative composition and formulae of scapolite from elecrtron microprobe analyses

Sample No.	01	02	03	04	05		06	07	08		09		10	11	12			13
	TAN-unk	TAN-SIN	TAN-MPW	SRI-unk	JPN-KSG		TAN-MOR	SRI-BAD	MYA		JPN-KBS		MOZ	NOR	PRK			BRA
Oxide					Ma-rich	Me-rich			Ma-rich	Me-rich	Ma-rich	Me-rich			Ma-rich	Me-rich	Ma-rich	Me-rich
Na_2O	12.77	12.21	11.57	11.56	11.21	6.16	10.32	9.15	9.28	8.44	9.41	7.63	9.27	9.51	7.58	8.61	7.46	7.75
MgO	0.00	0.00	0.01	0.03	0.02	0.04	0.01	0.03	0.03	0.04	0.01	0.08	0.06	0.02	0.02	0.01	0.07	0.04
Al_2O_3	19.35	20.05	21.68	21.70	22.00	26.65	22.45	22.01	22.67	23.29	22.97	24.45	23.03	23.31	24.83	23.65	24.88	23.76
SiO_2	61.93	60.39	58.30	58.30	57.86	50.33	56.92	56.14	55.42	54.25	56.36	54.17	55.85	56.14	52.82	54.82	53.08	54.00
SO_3	0.30	0.27	0.44	0.17	0.14	0.14	0.54	0.14	0.21	0.25	0.12	0.10	0.29	0.21	0.15	0.12	0.13	0.69
Cl	4.00	3.83	3.63	3.67	3.28	1.62	3.40	3.18	3.04	2.63	3.34	2.52	3.19	2.94	2.23	3.02	2.59	2.74
K_2O	1.41	1.17	0.75	0.60	0.39	0.31	1.04	1.68	1.74	1.58	1.28	1.04	1.37	0.94	0.84	1.53	1.54	1.36
CaO	1.78	2.90	4.50	4.66	5.48	13.56	6.08	6.61	6.67	8.39	7.23	10.34	7.25	7.53	10.65	8.26	9.93	9.26
TiO_2	0.00	0.00	0.01	0.03	0.03	0.04	0.01	0.03	0.03	0.04	0.07	0.00	0.03	0.01	0.01	0.03	0.03	0.02
FeO	0.05	0.12	0.10	0.04	0.05	0.08	0.05	0.03	0.02	0.08	0.12	0.00	0.07	0.07	0.00	0.04	0.06	0.13
TOTAL	101.58	100.94	100.99	100.75	100.46	98.91	100.83	99.02	99.11	99.00	100.90	100.33	100.41	100.68	99.13	100.08	99.78	99.75
Total-O/Cl	100.68	100.07	100.17	99.92	99.72	98.55	100.07	98.30	98.42	98.40	100.15	99.76	99.69	100.01	98.62	99.40	99.19	99.13
Cation number																		
Na	3.505	3.382	3.211	3.206	3.113	1.754	2.880	2.595	2.628	2.403	2.624	2.139	2.599	2.645	2.149	2.422	2.107	2.199
Mg	0.000	0.000	0.001	0.006	0.005	0.008	0.002	0.007	0.007	0.009	0.002	0.018	0.012	0.005	0.004	0.002	0.015	0.009
Al	3.229	3.374	3.657	3.659	3.714	4.611	3.808	3.793	3.903	4.032	3.894	4.167	3.925	3.943	4.278	4.045	4.271	4.098
Si	8.771	8.626	8.343	8.341	8.286	7.389	8.192	8.207	8.097	7.968	8.106	7.833	8.075	8.057	7.722	7.955	7.729	7.902
S	0.032	0.029	0.047	0.018	0.015	0.015	0.058	0.016	0.023	0.028	0.013	0.011	0.032	0.023	0.016	0.013	0.014	0.076
Cl	0.960	0.927	0.881	0.889	0.795	0.403	0.830	0.789	0.753	0.655	0.814	0.618	0.781	0.716	0.553	0.744	0.640	0.680
K	0.255	0.213	0.138	0.109	0.072	0.057	0.192	0.313	0.325	0.297	0.236	0.191	0.252	0.173	0.156	0.282	0.285	0.254
Ca	0.270	0.443	0.690	0.714	0.841	2.133	0.938	1.036	1.044	1.320	1.114	1.602	1.123	1.157	1.669	1.284	1.550	1.452
Ti	0.000	0.000	0.001	0.003	0.003	0.004	0.001	0.003	0.003	0.004	0.007	0.000	0.004	0.002	0.001	0.004	0.003	0.002
Fe	0.005	0.000	0.001	0.004	0.004	0.006	0.001	0.005	0.005	0.010	0.006	0.000	0.007	0.005	0.009	0.005	0.004	0.006
Calc. CO_3	0.028	0.060	0.052	0.092	0.177	0.536	0.099	0.199	0.182	0.321	0.199	0.373	0.184	0.224	0.402	0.243	0.294	0.229
ΣM	4.034	4.038	4.041	4.039	4.036	3.959	4.013	3.957	4.008	4.039	3.982	3.950	3.993	3.985	3.987	3.996	3.961	3.920
ΣA	1.019	1.017	0.981	0.999	0.987	0.954	0.988	1.003	0.959	1.005	1.026	1.001	0.996	0.963	0.971	0.999	0.948	0.984
X_{An}	7.6	12.5	21.9	22.0	23.8	53.7	26.9	26.4	30.1	34.4	29.8	38.9	30.8	31.4	42.6	34.8	42.4	36.6
X_{Me}	6.8	11.0	17.2	18.0	21.1	54.3	23.5	26.6	26.4	33.2	28.3	41.0	28.7	29.3	42.2	32.4	39.7	37.5

substitutional trends has not been well-established.

Many researchers have reported that the symmetry of scapolite depends on the chemical composition. The compositions near both end-members are consistent with the space group $I4/m$, and the intermediate compositions have the space group $P4_2/n$ (e.g., Lin and Burley 1973; Oterdoom and Wenk 1983; Teertstra and Sherriff 1996; Sokolova et al. 1996; Sherriff et al. 1998, 2000). $P4_2/n$ introduces Al/Si ordering into the scapolite structure (Teertstra and Sherriff 1996, 1997; Oterdoom and Wenk 1983). The Al/Si ordering was investigated in detail in a series of studies using nuclear magnetic resonance (NMR) spectroscopy (Sokolova et al. 1996; Sherriff et al, 1998, 2000). That series of studies showed that the three subseries established by Teertstra and Sherriff (1996, 1997) are associated with changes in space group and trends in cell parameters. These workers also carefully examined the occupancy of the tetrahedral site in each series. In contrast, Phakey and Ghose (1972), Buseck and Iijima (1974), and Hassan and Buseck (1988) reported that the intermediate composition has the space group $P4/m$ on the basis of electron diffraction patterns obtained from transmission electron microscopy (TEM). The space group $P4/m$ introduces Cl/CO_3 ordering into the scapolite structure.

In this study, we obtained 28 samples from various occurrences and investigated the chemical zoning in several samples. Symmetry properties and microstructure were also observed with the TEM. The purpose of this study is to examine the chemical substitutions of scapolite and the relationship between composition and symmetry.

EXPERIMENTS METHODS

Samples

A total of 28 natural scapolites were investigated in the present study. Petrographic thin sections were prepared for all samples. Sample descriptions are given in Appendix 1.

Chemical analysis

Chemical compositions of all samples were measured using a scanning electron microscope (SEM) and an energy dispersive X-ray spectrometer (EDX) system (HITACHI S-3000H + HORIBA EMAX7000) operating at 20kV and a beam current of 0.3 nA. Although Vanko and Bishop (1982) reported that the electron beam may give incorrect totals for the light alkali elements of scapolite, no loss of counts was detected for the above condition.

The formulae of scapolites were calculated by normalizing Al+Si to 12. Although some Fe may be present as Fe^{3+} all Fe was assumed to be Fe^{2+}. However, because of the small amounts of total Fe the amount is not significant for calculating the formula. CO_3^{2-} is a major component of scapolite, but carbon is not detectable from the carbon-coated samples for EDX analyses. Therefore, CO_3^{2-} is calculated from the charge-balance: $2O + Cl + 2CO_3 + 2SO_4 = Na + K + 2Ca + 3Al + 4Si$, where $Al + Si = 12$ and $O = 24$.

It is important to have a means to compare compositions of various scapolites. X_{Me}% [Ca/(Na+K+Ca)] or X_{EqAn}% [(Al-3)/3] has been introduced by previous researchers to describe the chemical variations of scapolite. However, we propose that projection onto the "scapolite plane" is a more flexible and widely applicable method for comparing various samples because the relationships between Ca/Na, Al/Si, and Cl/CO_3 can also be introduced. Our data were transformed to the quaternary system (albite-anorthite-calcite-halite) by a least-squares method. Details of the transformation method are described in Appendix 2. In the transformation, monovalent cations, such as potassium (K), are counted as sodium (Na), and divalent cations are counted as calcium (Ca). Cl^- and CO_3^{2-} are also represented by monovalent and divalent anions respectively.

TABLE 1.–*continued*

14		15	16	17	18	19		20		21	22	23	24	25	26		27	28
JPN-MTT		ANTA-ONG	NEP	CAN-BL	MAD	JPN-KBT		CAN-GR		NAM	ANTA-LAN	SRI-PEL	ANTA-SIN	ANTA-OME	JPN-ABK		ANTA-KAS	ANTA-SKA
Ma-rich	Me-rich					Ma-rich	Me-rich	Ma-rich	Me-rich						Ma-rich	Me-rich		
8.09	5.95	6.59	7.61	6.33	5.58	6.04	3.93	4.51	3.71	3.73	3.31	2.96	3.21	2.92	2.72	1.99	1.95	1.27
0.00	0.14	0.05	0.03	0.07	0.07	0.07	0.06	0.09	0.12	0.23	0.24	0.16	0.09	0.04	0.08	0.12	0.07	0.12
23.42	24.79	24.16	24.41	24.83	24.76	25.89	27.60	26.07	26.98	26.40	27.20	26.85	27.56	27.73	27.91	28.88	29.65	29.70
55.37	51.94	51.80	53.06	51.56	50.62	50.78	47.41	48.32	47.32	47.22	47.34	46.51	45.73	45.26	45.63	43.48	43.73	41.81
0.01	0.09	0.10	0.12	1.38	2.99	0.10	0.08	1.98	2.18	0.20	0.20	0.09	2.33	2.32	0.12	0.09	0.06	0.07
2.90	2.07	2.48	2.12	1.74	1.76	1.38	0.57	0.35	0.26	0.89	0.94	0.04	0.02	0.01	0.49	0.10	0.10	0.10
1.26	0.98	1.45	0.40	0.90	1.19	0.58	0.37	0.35	0.36	0.72	0.84	0.28	0.07	0.13	0.62	0.18	0.12	0.10
8.77	12.06	10.58	10.75	12.03	12.53	13.30	16.60	15.64	16.89	16.19	16.67	18.13	17.94	18.25	17.97	19.75	20.17	21.02
0.01	0.03	0.03	0.03	0.03	0.07	0.03	0.03	0.02	0.00	0.05	0.03	0.04	0.04	0.04	0.00	0.01	0.03	0.02
0.03	0.08	0.09	0.06	0.11	0.19	0.12	0.16	0.00	0.01	0.17	0.19	0.40	0.22	0.21	0.02	0.18	0.19	0.21
99.86	98.12	97.32	98.58	98.98	99.76	98.29	96.81	97.32	97.83	95.80	96.96	95.47	97.21	96.91	95.56	94.79	96.07	94.43
99.21	97.66	96.76	98.10	98.58	99.36	97.98	96.68	97.24	97.78	95.59	96.75	95.46	97.20	96.90	95.45	94.76	96.05	94.41
2.270	1.707	1.911	2.165	1.821	1.627	1.727	1.143	1.327	1.092	1.109	0.968	0.883	0.955	0.871	0.807	0.598	0.577	0.386
0.000	0.031	0.011	0.007	0.016	0.016	0.015	0.012	0.021	0.026	0.053	0.053	0.038	0.021	0.009	0.019	0.027	0.017	0.029
3.992	4.320	4.256	4.219	4.344	4.388	4.504	4.883	4.664	4.823	4.766	4.845	4.858	4.984	5.032	5.026	5.269	5.330	5.469
8.008	7.680	7.744	7.781	7.656	7.612	7.496	7.117	7.336	7.177	7.234	7.155	7.142	7.016	6.968	6.974	6.731	6.670	6.531
0.001	0.010	0.012	0.013	0.153	0.337	0.011	0.009	0.226	0.249	0.023	0.023	0.010	0.268	0.268	0.013	0.010	0.007	0.008
0.711	0.519	0.628	0.526	0.439	0.448	0.345	0.144	0.090	0.067	0.231	0.241	0.011	0.006	0.002	0.127	0.027	0.025	0.026
0.233	0.185	0.276	0.075	0.170	0.228	0.109	0.072	0.068	0.069	0.141	0.163	0.055	0.013	0.025	0.121	0.035	0.023	0.019
1.358	1.911	1.694	1.689	1.914	2.018	2.104	2.670	2.544	2.744	2.657	2.699	2.983	2.948	3.011	2.942	3.276	3.297	3.518
0.001	0.003	0.003	0.003	0.003	0.008	0.004	0.004	0.002	0.000	0.006	0.003	0.005	0.004	0.004	0.000	0.001	0.003	0.003
0.009	0.006	0.007	0.005	0.007	0.006	0.011	0.014	0.008	0.002	0.008	0.012	0.009	0.008	0.008	0.003	0.009	0.010	0.009
0.268	0.454	0.352	0.439	0.387	0.221	0.613	0.782	0.660	0.647	0.807	0.742	1.044	0.696	0.695	0.828	0.960	0.936	0.994
3.871	3.839	3.898	3.941	3.929	3.895	3.967	3.911	3.967	3.934	3.969	3.895	3.967	3.945	3.924	3.892	3.945	3.923	3.961
0.981	0.983	0.991	0.977	0.979	1.006	0.969	0.936	0.976	0.962	1.061	1.007	1.065	0.971	0.965	0.969	0.997	0.968	1.029
33.1	44.0	41.9	40.6	44.8	46.3	50.1	62.8	55.5	60.8	58.9	61.5	61.9	66.1	67.7	67.5	75.6	77.7	82.3
35.3	50.8	44.0	43.2	49.4	52.5	53.7	69.0	64.9	70.5	68.5	71.0	76.4	75.5	77.2	76.2	84.0	84.7	89.8

TEM observations

Electron diffraction and microstructural analyses were performed on 21 samples (No. 01–10, 13–14, 17–23, 27–28) with a TEM (HITACHI H-8000 and JEOL JEM-2000FXII) operating at 200kV. TEM specimens were prepared by crushing in acetone for homogeneous samples, or made from petrographic thin sections polished on both sides by ion bombardment for inhomogeneous ones. Areas corresponding to the entire compositional range in inhomogeneous samples were not fully observed because it is difficult to thin a particular selected area by the ion bombardment method.

We will take a close look at the three spaces group, $I4/m$, $P4_2/n$, and $P4/m$, proposed in previous studies. Reciprocal-space observations of scapolite reveal that the reflections can be divided into four types:

1. Type *a*: (*hkl*), $h+k+l$ = even. These occur in all the space groups considered.

2. Type *b*: (*hkl*), $h+k+l$ = odd. These are incompatible with the *I*-lattice in space group $I4/m$.

3. Type *c*: (00*l*), l = odd. These are incompatible with the 4_2 screw axis in space group $P4_2/n$.

4. Type *d*: (*hk*0), $h+k$ = odd. These are incompatible with the *n* glide plane in space group $P4_2/n$.

We sought to observe these types of reflections, and also checked for the possibility of multiple diffraction.

A few researchers (Phakey and Ghose 1972; Hassan and Buseck 1988) reported the presence of anti-phase boundaries (APBs) in intermediate composition scapolites. In the present study, the samples that have *P*-lattice symmetry were observed by the dark-field (DF) method using type *b* reflections to look for similar anti-phase domains.

RESULTS

Chemical compositions of samples

Projection onto the "scapolite plane." Representative chemical compositions of 28 samples are shown in Table 1.The compositional range in the present ranges varies from X_{Me} = 7 to = 90% or from X_{EqAn} = 8 to 82%. For inhomogeneous samples, both the Me-richest and Ma-richest data are given in the Table 1. The sum of M cations and the sum of A anions are close to the ideal values of 4 and 1, respectively. Deviations from the ideal values are probably due to some OH^-, H^+, or H_2O, whose importance were pointed out by Teertstra and Sherriff (1997). However, the deviations of the present data are small, and we do not need to consider such factors.

Figure 2 shows the projection of all samples onto the "scapolite plane." The scapolites of the present study are roughly distributed between the two end-members, marialite and meionite, and show large compositional overlap with analyses published in previous studies. The compositions near the lower right (anorthite + halite) and the upper left (albite + calcite) corners on the scapolite plane are not observed, although they are theoretically possible for scapolite compositions. This trend seemingly agrees with those obtained by previous researchers. However, several samples (e.g., No. 05) are far from the trends proposed in previous studies.

Compositional variations in inhomogeneous samples. Chemical zoning should directly reflect the compositional trend during growth and reflect conditions of the growth environment. Particular attention was paid to the chemical zoning in inhomogeneous scapolite, especially the compositional variations within a single grain. As shown in Figure 2, several samples (Nos. 05, 09, 11, 12, 14, 19, 20, and 26) show significant inhomogeneity. For example, JPN-KBS (No. 09) shows remarkable oscillatory

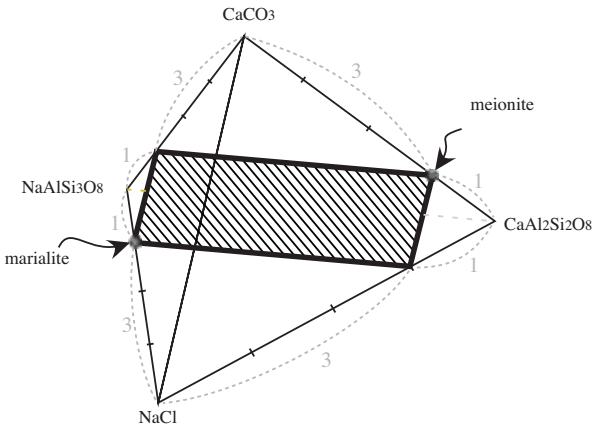

FIGURE 1. Albite-anorthite-halite-calcite quaternary system. The hachured plane, the "scapolite plane," denotes the plane of theoretically possible scapolite compositions.

zoning (Fig. 3). Even if zonal structures are not clear in backscattered electron images, they are prominent in cathodoluminescence (CL) images. A strong correlation between variations in Na, Ca, Si, Al (= 12 – Si), and Cl were observed.

Three particularly inhomogeneous samples, JPN-KSG (No. 05), JPN-KBS (No. 09), and JPN-KBT (No. 19) have very wide compositional variations. The range of compositions and the corresponding trends for these three samples are as follows:

(1) JPN-KSG (No. 05) = $Na_{3.30}Ca_{0.72}Al_{3.63}Si_{8.37}O_{24}Cl_{0.87}(CO_3)_{0.12}$ – $Na_{1.28}Ca_{2.66}Al_{4.98}Si_{7.02}O_{24}Cl_{0.24}(CO_3)_{0.70}$ $Na_{1.49}SiCl_{0.47}[Ca_{1.44}Al(CO_3)_{0.43}]_{-1}$

(2) JPN-KBS (No. 09) = $Na_{2.99}Ca_{1.02}Al_{3.86}Si_{8.14}O_{24}Cl_{0.88}(CO_3)_{0.15}$ – $Na_{1.94}Ca_{1.98}Al_{4.40}Si_{7.60}O_{24}Cl_{0.45}(CO_3)_{0.52}$ $Na_{1.91}SiCl_{0.79}[Ca_{1.75}Al(CO_3)_{0.69}]_{-1}$

(3) JPN-KBT (No. 19) = $Na_{1.99}Ca_{1.97}Al_{4.41}Si_{7.59}O_{24}Cl_{0.40}(CO_3)_{0.56}$ – $Na_{1.02}Ca_{2.85}Al_{4.98}Si_{7.02}O_{24}Cl_{0.07}(CO_3)_{0.84}$ $Na_{1.69}SiCl_{0.58}[Ca_{1.55}Al(CO_3)_{0.50}]_{-1}$

Each of these three compositional trends shows a wide variation and high linearity (Fig. 4).

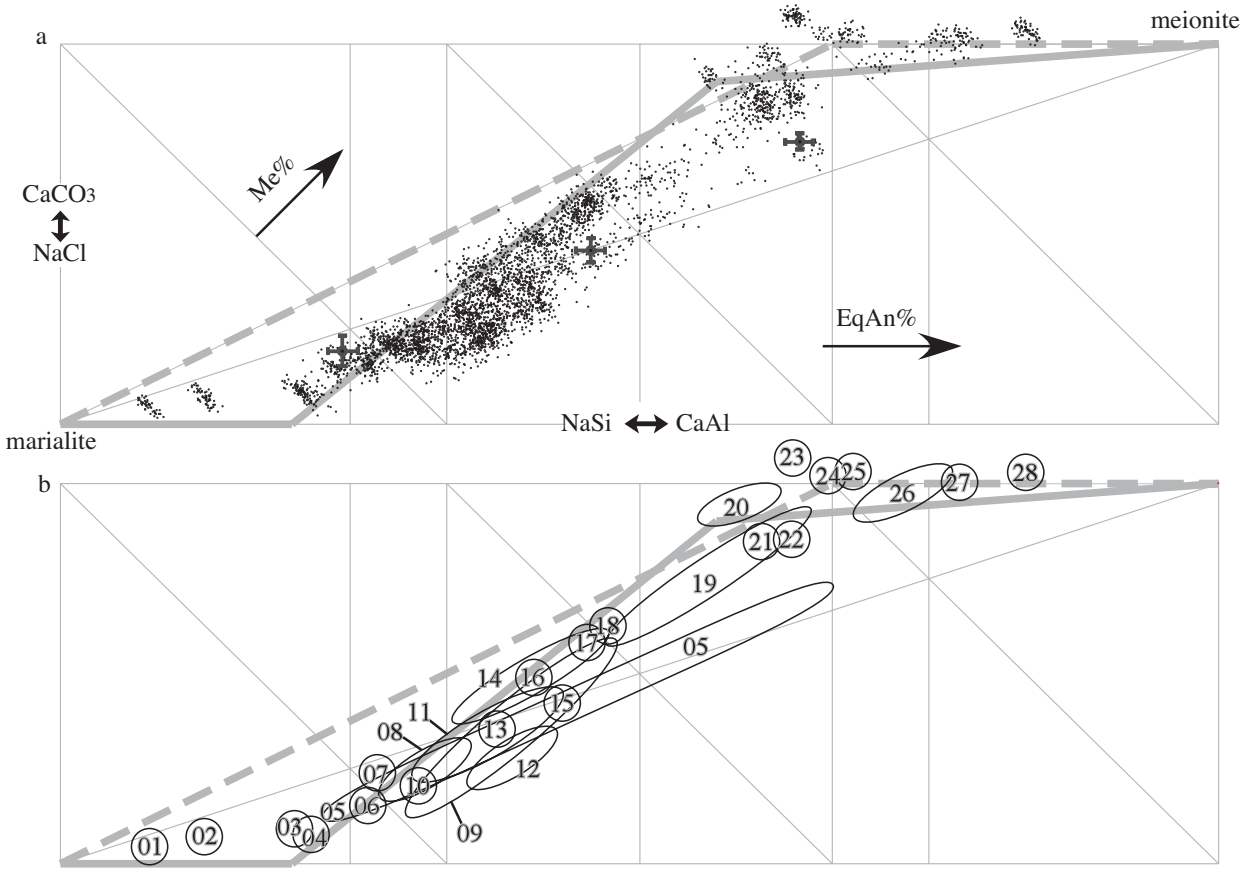

FIGURE 2. (**a**) Projection of all data onto the "scapolite plane." Error bars for three analyses are also shown. Dash and solid lines show the proposal for substitution trends by Evans et al. (1969) and Teertstra and Sherriff (1997), respectively. (**b**) A schematic representation of the chemical variation of each of the samples of the present study.

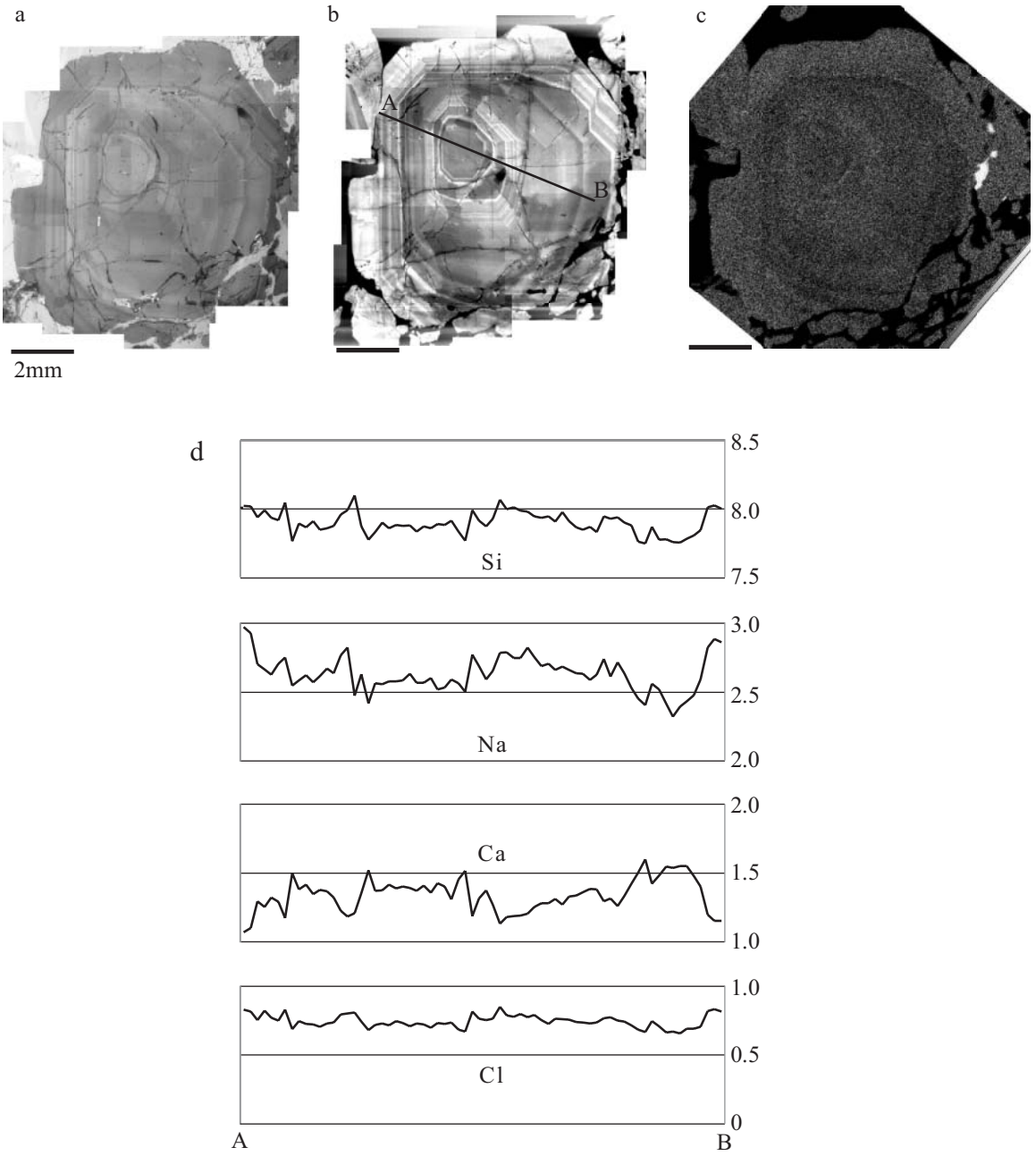

FIGURE 3. Zonal structure of scapolite sample JPN-KBS (No. 09). (**a**) Polarized microscope image (**b**) Cathodoluminescence image and (**c**) element concentration image calculated by combining concentrations of Na, Si, Cl, Ca, and Al. (**d**) Line profiles of concentrations of Na, Ca, Al, Si, and Cl.

Electron diffraction patterns and anti-phase domains of scapolite

In selected area electron diffraction (SAED) patterns, type *b* reflections are observed in all samples (Fig. 5a) except for three Ma-rich ones (No. 01-03). In the latter cases type *b* reflections are completely absent when observed from any zone axes, as shown in Figure 5b. Even the most Me-rich sample (No. 28) shows weak, but significant, type *b* reflections (Fig. 5c). The existence of type *b* reflections suggests a *P*-lattice symmetry.

It is difficult to judge whether type *c* reflections are completely absent because the type *c* reflections probably occur by multiple diffraction from type *b* reflections. However, even if type *c* reflections are observed (e.g., Fig. 5a), these reflections weaken and finally disappear (Fig. 5d) on tilting about the systematic rows for the purpose of eliminating the multiple diffractions. Therefore, we can say that type c reflections are essentially absent. Type *d* reflections in [001] patterns disappear completely (Fig. 5e) in all samples except for JPN-KBS (No. 09). In a small part of JPN-KBS, type *d* reflections in [001] patterns are observed (Fig. 5f), whereas in other parts these reflections are absent. Type *d*

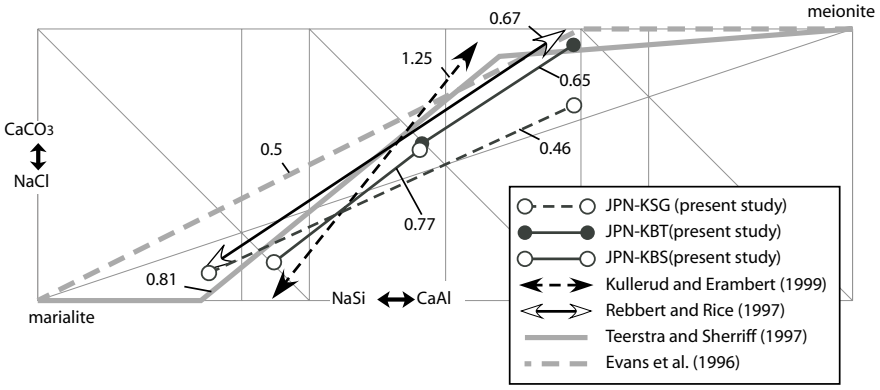

FIGURE 4. Various substitutional trends of the scapolite series. Inserted values mean a ratio of NaCl $(CaCO_3)_{-1}$ vs. NaSi $(CaAl)_{-1}$.

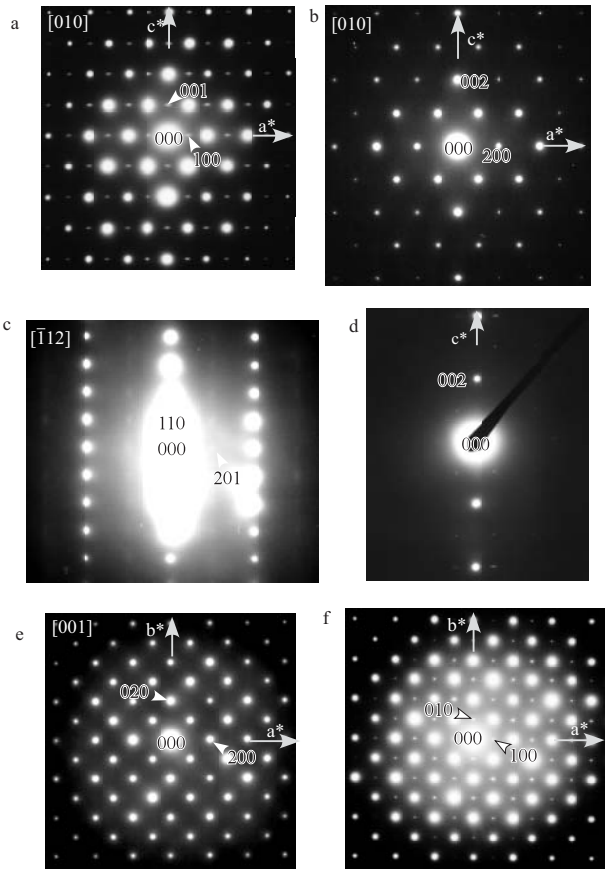

FIGURE 5. (**a**) Type *b* reflections present in the [010] pattern of ANTA-LAN. The same results are found in samples No. 04-28. (**b**) Type *b* reflections disappear in the diffraction pattern of TAN-SIN. The same results are found in No. 01-03. (**c**) The most Me-rich sample (No. 28 ANTA-SKA) show type *b* reflections. (**d**) Type *c* reflections weaken on tilting about systematic rows containing these spots. The same results are seen in samples No. 04-28. (**e**) Type *d* reflections disappear in the [001] pattern of TANZ-MOR. The same results are found in all observed samples except for JPN-KBS (No. 09). (**f**) Type *d* reflections are clearly observed in the [001] pattern of JPN-KBS.

reflections in [001] patterns cannot occur by multiple diffraction from type *b* reflections. The existence of type *d* reflections suggests an absence of an *n* glide plane.

In dark-field observation using type *b* reflections, APBs could be imaged (Figs. 6a–d) in all *P*-lattice samples. The presence of APBs is likely to be due to the *I*-*P* phase transition. All samples that have a *P*-lattice symmetry show APBs, and therefore we infer that they had *I*-lattice symmetry at the time of their formation. Sample CA-BL (No. 17) shows smoothly curved and sharp APBs, and the anti-phase domains (APDs) are 2 μm wide (Fig. 6b), which are similar to those observed by Phakey and Ghose (1972). Sample JPN-KBT (No. 19) shows fuzzy and irregular APBs, and the APDs are tens of nanometers wide (Fig. 6c), which are similar to those observed by Oterdoom and Wenk (1983). It is difficult to relate the compositions directly to the domain sizes, but Me-rich samples commonly have small domains. The variation in observed domain sizes should be related to the cooling rate near the temperature of the phase transition and the presence or absence of water.

The dark-field observation of sample JPN-KBS using the type *d* reflections shows a lamellar structure along (100) several tens of nanometers wide (Fig. 6e). The existence of type *d* reflections suggests an absence of an *n* glide plane. Phakey and Ghose (1972) observed type *c* and *d* reflections and concluded that possible space groups for their sample (Me = 37%) are *P*4 and *P*4/*m*, which support Cl/CO_3 ordering. Hassan and Buseck (1988) also reported type *c* and *d* reflections that occur as diffuse spots in the zero-order Laue zone. On a sub-micrometer scale, the symmetry may be modified and lose the *n*-glide plane. But this fact is not the point in question, because the type *d* reflections could be observed from only one sample in the present 28 samples, and even in that sample, these reflections are absent in most parts of the specimen. There is no need to go into details about this texture in the following discussion.

DISCUSSION

Compositional variation of scapolite solid solutions

Chemical analyses in the present study show that the compositions of various samples lie widely scattered between the marialite – meionite components within the "scapolite plane." The formulae $3[NaAlSi_3O_8] + [CaCO_3]$ and $3[CaAl_2Si_2O_8] + [NaCl]$, which are theoretically possible, are not observed. Chamberlain et al. (1985) suggested that local charge balance between alkali cations and volatile anions governs the composition of scapolites. The local charge balance may loosely constrain the trend along

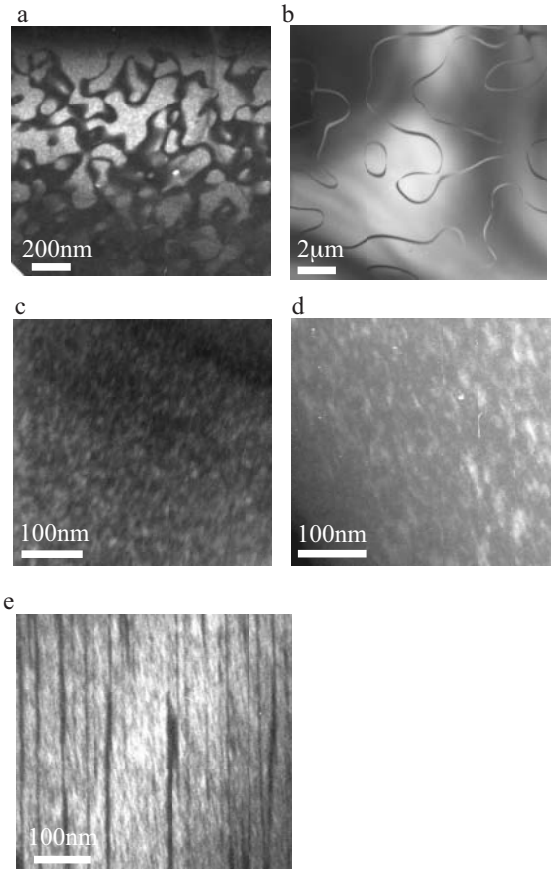

FIGURE 6. a–d Dark-field TEM observation using type *b* reflections. (**a**) No. 07 SRI-BAD. (**b**) No. 17 CA-BL. (**c**) No. 19 JPN-KBT. (**d**) No. 20 ANTA-LAN. Anti phase domain structures were observed in other *P*-lattice phase samples. (**e**) No.09 JPN-KBS. Dark-field TEM observation using the type *d* reflections shows a lamellae structure.

the marialite – meionite join.

The chemical zoning should directly reflect the crystallization environment during its growth. As mentioned before, at least three of the present samples (JPN-KBS, JPN-KSG, and JPN-KBT) show remarkable chemical zoning and several different linear trends could be derived to describe the compositional variations as follows: for sample JPN-KSG, $Na_{1.49}SiCl_{0.47}[Ca_{1.44}Al(CO_3)_{0.43}]_{-1}$; JPN-KBT, $Na_{1.69}SiCl_{0.58}[Ca_{1.55}Al(CO_3)_{0.50}]_{-1}$; and for JPN-KBS, $Na_{1.91}SiCl_{0.79}[Ca_{1.75}Al(CO_3)_{0.69}]_{-1}$. Three samples have highly linear paths, rather than zigzag ones, and these three paths intersect each other. These three samples are from skarn rocks from different localities, and likely formed at similar pressures of a few kbar although exact *P-T* conditions were not determined.

Kullerud and Erambert (1999) suggested that significant differences in the solid solution probably occur in scapolite from different occurrences, and that the extent of coupling between NaSi $(CaAl)_{-1}$ and NaCl $(CaCO_3)_{-1}$ is dependent on the metamorphic conditions (e.g., *P* and *T*). They reported that the exchange reaction of scapolite formed under high-pressure conditions of 8 to 11 kbar at 550 to 620 ºC, is estimated to be $Na_{1.9}Si_{0.8}Cl[Ca_{1.9}Al_{0.8}(CO_3)]_{-1}$. The compositional trend of their samples is also drawn in Figure 4 and has a significantly higher slope than the other trends in the scapolite plane. This result suggests a possibility that the slope of the substitution trend depends upon the pressure during crystal growth. One other trend reported by Rebbert and Rice (1997) is, however, in conflict with the idea of pressure dependence. Their samples were collected from a regionally metamorphosed terrane (450–670 ºC, 3.5–6 kbar), and should have formed under higher pressure conditions than those of the present three samples from skarn rocks. Nonetheless, their trend nearly overlaps with that of JPN-KBT (No. 19). This result indicates that the compositional variation of scapolite depends not only upon the metamorphic pressure and temperature, but also on the other factors related to the crystallization environment such as the activity of the volatiles of the equilibrium fluid. For example, Jiang et al. (1994) pointed out that the Cl content of scapolite is strongly controlled by the NaCl activity of the equilibrium fluid.

Phase transition of scapolite

The SAED results depend on neither sizes of the selected area nor positions in each sample, and they are not likely due to the local symmetry. The systematical extinction of type *c* and *d* reflections (Figs. 5d and 5e) in the *P*-lattice samples supports the presence of an *n* glide plane normal to the *c*-axis and a 4_2 screw axis parallel to the *c*-axis respectively. The presence of the *n* glide and the 4_2 screw axis suggests a space group of $P4_2/n$ rather than $P4/m$. Moreover, the presence of type *b* reflections in almost Cl-free samples (Nos. 23, 27, and 28) suggests Al/Si ordering rather than Cl/CO_3. It is, therefore, reasonable to suggest that the *P*-lattice samples in the present study have a $P4_2/n$ space group.

Type *b* reflections appear in the three Ma-rich samples (No. 01 TANZ-unk, 02 TANZ-SIN, and 03 TANZ-MPW). These results suggest that the three samples have a body-centered (*I*-lattice) symmetry and the results are consistent with a space group of $I4/m$. SRI-unk (No. 04 $[Na_{3.29}Ca_{0.74}][Al_{3.62}Si_{8.38}]Cl_{0.91}(CO_3)_{0.12}$) has a space group of $P4_2/n$ although it has the very near the composition of TANZ-MPW (No. 03, $[Na_{3.34}Ca_{0.74}][Al_{3.61}Si_{8.39}]Cl_{0.89}(CO_3)_{0.16}$). This value agrees with the $[Al_{3.6}Si_{8.4}O_{24}]$ value (X_{EqAn} = 20%) determined as the *I-P* phase boundary on the Ma-rich side by Teertstra and Sherriff (1997). Results for samples with X_{EqAn} <20% are compatible with a space group of $I4/m$ in low-temperature conditions (Fig. 7).

On the other hand, there is a considerable disagreement about the *I-P* phase boundary on the Me-rich side between the proposal of Teertstra and Sherriff (1997) and our present study. Even the most Me-rich sample (28 ANTA-SKA: X_{EqAn} = 82% and X_{Me} = 90%) used in the present study has a *P*-lattice, whereas a composition of $[Al_{4.7}Si_{7.3}O_{24}]$ (X_{EqAn} = 57%) was reported as the *I-P* phase boundary on the Me-rich side by Teertstra and Sherriff (1997). As clearly seen in Figure 7, there are the similar disagreements on this point between the proposal by Teertstra and Sherriff (1997) and the data by Oterdoom and Wenk (1983) and Lin and Burley (1973). The presence of APDs strongly shows that the present Me-rich scapolites had formed originally as $I4/m$ at higher

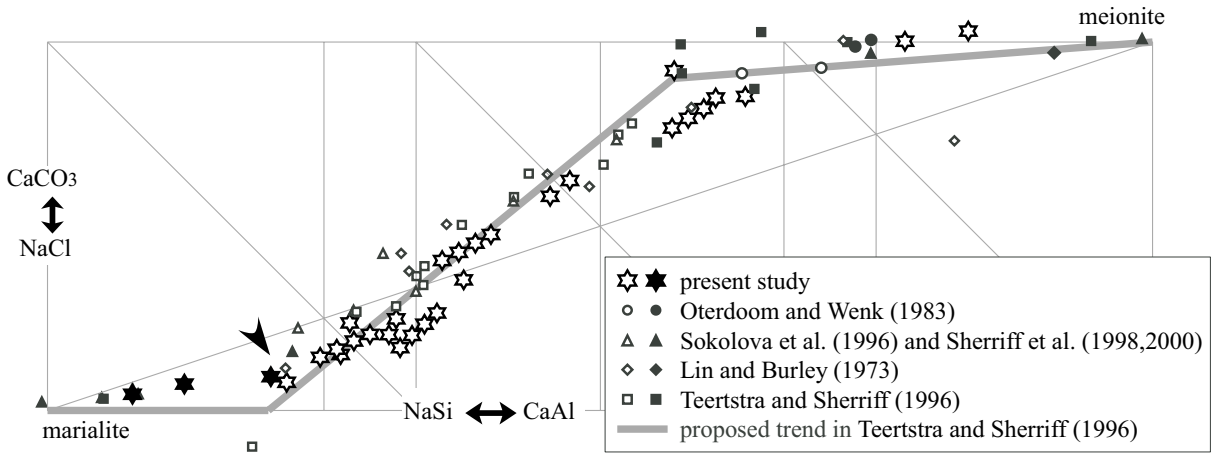

FIGURE 7. The relation between the composition and symmetry. Open and solid patterns show *P*- and *I*-lattice phase respectively. The solid arrow indicates the suggested location of the *I*-*P* phase boundary on the Ma-rich side. The boundary on the Me-rich side is uncertain.

temperatures and then transformed into $P4_2/n$ during cooling. In the case of very rapid cooling, there might be a possibility that the *I*-*P* phase transition did not occur and the high-temperature $I4/m$ form persists metastably at lower temperature. Therefore, the *I*-*P* phase boundary on the Me-rich side probably depends on their occurrences.

ACKNOWLEDGMENTS

The authors thank A. Harada, S. Yamada, M. Bunno, and Y. Hiroi who kindly provided samples for this study. The authors are grateful to S. Wallis for improvements to the manuscript. The authors are also grateful to T. Duffy and two anonymous reviewers for their thoughtful comments and constructive suggestions.

REFERENCES CITED

Buseck, P.R. and Iijima, S. (1974) High resolution electron microscopy of silicates. American Mineralogist, 59, 1–24.

Chamberlain, P.C., Docka, J.A., Post, J.E., and Burnham, C.W. (1985). Scapolite: Alkali atom configurations, antiphase domains and compositional variations. American Mineralogist, 70, 134–140.

Evans, B.W., Shaw, D.M., and Haughton, D.R. (1969) Scapolite stoichiometry. Contributions to Mineralogy and Petrology, 24, 293–305.

Hassan, I. and Buseck, P.R. (1988) HRTEM characterization of scapolite solid solutions. American Mineralogist, 73, 119–134.

Hiroi, Y. (1990) High-pressure and low-pressure mineral assemblages at the same outcrop near Yokokawa, Abukuma metamorphic terrane, Japan–Evidence for unique metamorphic evolution. Journal of Mineralogy, Petrology, and Economic Geology, 85, 207–222.

Hiroi, Y., Shiraishi, K., Nakai, Y., Motoyoshi, Y., and Katsushima, T. (1987) Progressive metamorphism of calc-silicate rocks from the Prince Olav and Sôya Coasts, east Antarctica. Proceedings of the NIPR Symposium on Antarctic Geosciences No. 1, 73–97.

Jiang, S.Y., Palmer, M.R., Xue, C.J., and Li, Y.H. (1994) Halogen-rich scapolite-biotite rocks from the Tongmugou Pb-Zn deposit, Qinling, north-western China: Implications for the ore-forming process. Mineralogical Magazine, 58, 543–552.

Kullerud, K. and Erambert, M. (1999) Cl-scapolite, Cl-amphibole, and plagioclase equilibra in ductile shear zones at Nusfjord, Lofoten, Norway: Implications for fluid compositional evolution during fluid-mineral interaction in the deep crust. Geochimica et Cosmochimica Acta, 63, 3829–2844.

Lin, S.B. and Burley, B.J. (1973) On the weak reflections violating body-centered symmetry in scapolites. Tschermaks Mineralogische und Petrographische Mitteilungun Dritte Folge, 20, 28–44.

Maruyama, S., Liou, J.G., and Suzuki, K. (1982) The peristerite gap in low-grade metamorphic rocks. Contributions to Mineralogy and Petrology, 81, 268–276.

Moecher, D.P. and Essene, E.J. (1990) Phase equilibra for calcic scapolite, and implications of variable Al-Si disorder for *P*-*T*, *T*-X_{CO_2}, and a-*X* relations. Journal of Petrology, 31, 997–1024.

———(1991) Calculation of CO_2 activities using scapolite equilibria: constraints on the presence and composition of a fluid phase during high grade metamorphism. Contribution to Mineralogy and Petrology, 108, 219–240.

Oterdoom, W.H. and Wenk, H.R. (1983) Ordering and Composition of scapolite: Field observation and structural interpretations. Contribution to Mineralogy and Petrology, 83, 330–41.

Phakey, P.P. and Ghose, S. (1972) Scapolite: Observation of anti-phase domain structure. Nature Physical Science, 238, 78–80.

Rebbert, C.R. and Rice, J.M. (1997) Scapolite-plagioclase exchange: Cl-CO_3 scapolite solution chemistry and implications for peristerite plagioclase. Geochimica et Cosmochimica Acta, 61, 555–567.

Sherriff, B.L., Sokolova, E.V., Kavalov, Yu.K., Teertstra, D.K., Kunath, G., Goetz, S., and Jäger, C. (1998) Intermediate scapolite: ^{29}Si MAS and ^{27}Al SATRAS spectroscopy and Rietveld structure-refinement. The Canadian Mineralogist, 36, 1267–1283.

Sherriff, B.L., Sokolova, E.V., Kavalov, Yu.K., Jenkins, D.M., Kunath-Fandrei, G., Goetz, S., Jäger, C., and Schneider, J. (2000) Meionite: ^{29}Si MAS and ^{27}Al SATRAS spectroscopy, and comments on the marialite–meionite series. The Canadian Mineralogist, 38, 1201–1213.

Sokolova, E.V., Kabalov, Yu.K., Sherriff, B.L., Teertstra, D.K., Jenkins, D.M., Kunath-Fandrei, G., Goezt, S., and Jäger, C. (1996) Marialite: Rietveld structure-refinement and ^{29}Si MAS and ^{27}Al SATRAS spectroscopy. The Canadian Mineralogist, 34, 1039–1050.

Teertstra, D.K. and Sherriff, B.L. (1996) Scapolite cell-parameter trends along the solid-solution series. The American Mineralogist, 81, 169–180.

———(1997) Substitutional mechanism, compositional trends and the end-member formulae of scapolite. Chemical Geology, 136, 233–260.

Teertstra, D.K., Schindler, M., Sherriff, B.L., and Hawthorne, F.C. (1999) Silvianite, a new sulfate-dominant member of the scapolite group with an Al-Si composition near the $I4/m$–$P4_2/n$ phase transition. Mineralogical Magazine, 63, 321–329.

Vanko, D.A. and Bishop, F.C. (1982) Occurrence and origin of marialitic scapolite in the Humboldt Lopolith, N.W. Nevada. Contributions to Mineralogy and Petrology, 81, 277–289.

MANUSCRIPT RECIVED MARCH 24, 2003
MANUSCRIPT ACCEPTED OCTOBER 8, 2003
MANUSCRIPT HANDLED BY THOMAS DUFFY

APPENDIX 1. SAMPLES

(Sample numbers are sorted by X_{Me})

01. TAN-unk is a transparent, violet colored crystal from TANZANIA.

02. TAN-SIN is a transparent, light violet colored gem scapolite from Singida, Northern Tanzania.

03. TAN-MPW is a transparent, deep violet colored crystal from Mpwapwa, Eastern Tanzania.

04. SRI-unk is a transparent, violet, gem-quality scapoltie from Sri Lanka.

05. JPN-KSG is from a dolomite-skarn, Kasuga area, Gihu prefecture, Japan. The geologic setting in this area was studied

by Maruyama et al. (1982).

06. TAN-MOR is a transparent, light yellow colored, gem-quality scapolite from Morongoro located in southeast Tanzania.

07. SRI-BAD is a transparent, light yellow crystal from Badulla, located in Southern Sri Lanka.

08. MYA is from a transparent, colorless scapolite from Mogok, Myanmar.

09. JPN-KBS is skarn from the Kobushi mine, Minamisaku area, Nagano prefecture, Japan.

10. MOZ is a transparent, colorless polished jemstone from Mozambique.

11. NOR is from Harmrefjell, Eikeren, Norway. NOR is an assemblage of opaque, white crystals.

12. PRK is from a skarn, Holkol, Hwanghaebukto, Democratic People's Republic of Korea.

13. BRA is a transparent, light yellow scapolite from Aracruz, located in eastern Brazil.

14. JPN-MTT is from a skarn, Mitate mine, Nishiusuki area, Miyazaki prefecture, Japan.

15. ANTA-ONG is from eastern Ongule Island, Antarctic.

16. NEP is from Dading located in eastern Nepal.

17. CAN-BL is a white impure colored, pillar-shaped scapolite from Bear Lake, Quebec, Canada.

18. MAD is an almost transparent, yellow colored crystal from Madagascar.

19. JPN-KBT is from a skarn, Kabuto area, Mie prefecture, Japan. KBT is an opaque, white scapolite.

20. CAN-GR is from Grenville, Quebec, Canada. CAN-GR is an assemblage of white, opaque crystals.

21. NAM is a white opaque scapolite from Namibia.

22. ANTA-LAN is from a metamorphosed calc-silicate rock, Langhovde, Lützow-holm complex in Sôya Coast, East Antarctic. Hiroi et al. (1987) studied the thermal structure and metamorphic conditions of the Lützow-holm complex including the areas of Langhovde (this sample), Sinnan Rock (No. 25), Cape Omega (No. 24), Kasumi Rock (No. 27), and Skarvsnes (No. 28).

23. SRI-PEL is a white opaque scapolite from Pelmadulla, located in the south-west of Sri Lanka.

24. ANTA-OME is from a metamorphosed calc-silicate rock (identical to specimen No. 770804 in Hiroi et al. 1987), from Cape Omega, Lützow-holm complex in Prince Olav Coast, East Antarctic.

25. ANTA-SIN is from metamorphosed calc-silicate rock (identical to specimen No. 81020906C in Hiroi et al. 1987) from Shinnan Rock, Lützow-holm complex in Prince Olav Coast, East Antarctic.

26. JPN-ABK is from a calc-silicate rock, Abukuma metamorphic terrane, Fukushima prefecture, Japan. Scapolite is present as a relic. The description of the locality and metamorphic evaluation are given in Hiroi (1990) and our samples are identical to specimen No. 84081508 in his paper.

27. ANTA-KAS is from a metamorphosed calc-silicate rock (identical to specimen No. 79020412 in Hiroi et al. 1987), Kasumi Rock, Lützow-holm complex in Prince Olav Coast, East Antarctic.

28. ANTA-SKA is from a metamorphosed calc-silicate rock (identical to specimen No. 84012801 in Hiroi et al. 1987), Skarvsnes, Lützow-holm complex in Sôya Coast, East Antarctic.

Appendix 2. The method of transformation atomic ratios into quaternary

If scapolite stoichiometry is shown as an exact quaternary in the system of albite-anorthite-halite–calcite, the relation between atomic ratio and component ratio is as follows.

$A_{Na}:A_{Ca}:A_{Si}:A_{Al}:A_{Cl} = C_{Ab} + C_{Hal}:C_{An} + C_{CC}:3C_{Ab} + 2C_{An}:C_{Ab} + 2C_{An}:C_{Hal}$.

where A_x is cation or anion ratio of x, C_y being components ratio of y.

When we obtain the atomic ratio $A^*_{Na}:A^*_{Ca}:A^*_{Si}:A^*_{Al}:A^*_{Cl}$ from the experimental value, the best estimated C must be to minimize Δ^2, which is the sum of weighted squares of deviation between A and A^*. Then, Δ^2 is as follows.

$\Delta^2 = \underline{\Delta}\cdot W\cdot\Delta\,| = (\underline{C}\cdot\tilde{Q} - \underline{A})\cdot W\cdot(Q\cdot C| - A|)$.

"_" and "|" represent row and column vectors respectively. The Q is a matrix expressed by

$$Q = \begin{pmatrix} 1 & 0 & 1 & 0 \\ 0 & 1 & 0 & 1 \\ 3 & 2 & 0 & 0 \\ 1 & 2 & 0 & 0 \\ 0 & 0 & 1 & 0 \end{pmatrix}$$

and $\tilde{Q}$ is the transposed matrix of Q.

The weight parameter W is a diagonal matrix with five diagonal elements; W_{Na}, W_{Ca}, W_{Si}, W_{Al}, and W_{Cl}. W_x is the reciprocal of square of the error for A_x.

When Δ^2 has the least value, derivative of Δ^2 by C is zero;

$$\partial\Delta^2 = \partial\underline{C}\cdot\tilde{Q}\cdot W\cdot(Q\cdot C| - A|) + (\underline{C}\cdot\tilde{Q} - \underline{A})\cdot W\cdot Q\cdot\partial C| =$$

$$2\partial\underline{C}(\tilde{Q}\cdot W\cdot Q\cdot C| - \tilde{Q}\cdot W\cdot A|) = 0$$

and then

$\tilde{Q}\cdot W\cdot Q\cdot C| - \tilde{Q}\cdot W\cdot A|) = 0$.

Thus we can write the best estimated C as

$C| = (\tilde{Q}\cdot W\cdot Q)^{-1}\cdot\tilde{Q}\cdot W\cdot A|$.